JOURNAL OF GEOPHYSICAL RESEARCH, VOL. 97, NO. C2, PAGES 2379–2389, FEBRUARY 15, 1992

The Effect of Small-Wave Modulation on the Electromagnetic Bias

ERNESTO RODRÍGUEZ, YUNJIN KIM, AND JAN M. MARTIN

Jet Propulsion Laboratory, California Institute of Technology, Pasadena

The effect of the modulation of small ocean waves by large waves on the physical mechanism of the electromagnetic (EM) bias is examined by conducting a numerical scattering experiment which does not assume the applicability of geometric optics. The modulation effect of the large waves on the small waves is modeled using the principle of conservation of wave action and includes the modulation of gravity-capillary waves. The frequency dependence and magnitude of the EM bias is examined for a simplified ocean spectral model as a function of wind speed. These calculations allow us to assess the validity of previous assumptions made in the theory of the EM bias, with respect to both scattering and hydrodynamic effects. We find that the geometric optics approximation is inadequate for predictions of the EM bias at typical radar altimeter frequencies, while the improved scattering calculations provide a frequency dependence of the EM bias which is in qualitative agreement with observation. We also find that, for typical wind speeds, the EM bias contribution due to small-wave modulation is of the same order as that due to modulation by the nonlinearities of the large-scale waves.

1. INTRODUCTION

It has been observed experimentally that for normal incidence, the reflection of radar pulses is stronger from ocean wave troughs than from wave peaks [*Yaplee et al.*, 1971; *Walsh et al.*, 1989 and personal communication, 1991; *Melville et al.*, 1991 and personal communication, 1990]. This causes the mean electromagnetic level of the ocean to be biased low relative to the true ocean mean level. This effect has been called the electromagnetic (EM) bias and is of importance to ocean altimetry.

Although the experimental characterization of the EM bias is not yet definitive, the general trends are clear. The magnitude of the bias increases with significant wave height (SWH), although the dependence may not be linear. To first order, the bias can be characterized as a percentage of SWH. The value of this percentage ranges from about 1% (for a radar wavelength of 0.8 cm), to about 6% (for a radar wavelength of 6 cm). The magnitude of the residual bias, after removal of a linear dependence on SWH, is an increasing function of wind speed for wind speeds up to approximately 10 m/s.

The first theoretical study of the EM bias was due to *Jackson* [1979], who used geometrical optics and the statistical height-slope correlation derived from the work of *Longuet-Higgins* [1963] to obtain the first theoretical predictions of the bias magnitude for a one-dimensional ocean with a Phillips spectrum [*Phillips*, 1980]. Subsequent work [*Srokosz*, 1986; *Barrick and Lipa*, 1985; R. E. Glazman and M. A. Srokosz, personal communication, 1991] has taken substantially the same approach and has sought to refine the calculations by introducing more realistic ocean spectral models. Recently, *Arnold et al.* [1991] have presented a model for the EM bias using physical optics, rather than geometric optics. Their model ignores modulations due to large-scale wave nonlinearities and assumes that all of the EM bias effect is due to small-wave modulations. A more detailed comparison of their results with those presented here must await a fuller presentation of their results.

Paper number 91JC02511.
0148-0227/92/91JC-02511$05.00

In spite of some qualitative success for this theoretical approach, there must remain some reservations about the assumptions used, both in the scattering and the hydrodynamic theory. The reservations concerning the scattering theory are clear. Geometric optics can be applied [*Tsang et al.*, 1985] to rough surfaces whose average radius of curvature is much larger than the electromagnetic wavelength. The radius of curvature of the ocean is dominated by the small-wave contribution and is typically centimetric. Figure 1 presents an example of the ratio of the electromagnetic wavelength to the mean radius of curvature for two typical radar wavelengths and for the spectral model assumed in this paper (see section 2). As can be seen, the geometric optics condition is not met. The standard way of dealing with this reservation is to assume that the surface seen by the radar is a filtered version of the true ocean surface [*Tyler*, 1976]. However, the nature of the filtering function is completely unspecified, rendering questionable any results derived by using this method.

A further reservation in the scattering theory has to do with the use of the "deep phase" approximation [*Tsang et al.*, 1985]: it is assumed that the root-mean-square (rms) surface height of the scattering patch is much larger than the electromagnetic wavelength. EM bias experiments have typically used very narrow beams, and the size of the scattering patch is of the order of a meter. For a typical ocean spectrum, the intrinsic height variation within such a patch, after an overall tilt (which changes the local incidence angle) has been removed, is usually of the order of 1 cm (see section 2 for more detailed calculations). Hence the deep phase assumption is also not justified for typical radar wavelengths.

The assumptions made for the hydrodynamic modeling cannot be faulted as clearly owing to our lack of a definitive theory for the nonlinear ocean. However, some of the assumptions require closer scrutiny. The scattering mechanism at nadir incidence is widely recognized to be dependent primarily on the slope variance of the scattering patch. As with the surface curvature, the surface slope is controlled by the high-frequency part of the spectrum. It has been noted, however [*Barrick and Lipa*, 1985], that the weak perturbation expansion used by the authors cited above breaks down

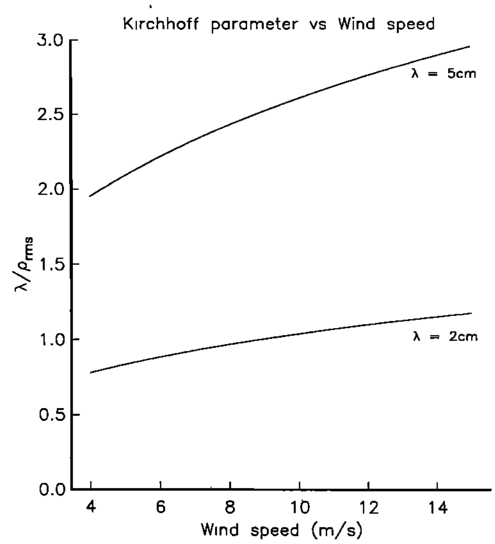

Fig. 1. Ratio of the electromagnetic wavelength to the mean radius of curvature for the two wavelengths considered in this paper and the spectral model presented in section 2. For the Kirchhoff approximation to be applicable, this ratio must be much less than 1.

for small waves. In any case, it is certainly true that gravity-capillary waves are responsible for much of the slope variance, and they are not included in the Longuet-Higgins model.

Two other factors that have the potential of contributing to the EM bias are ignored by this model. The first is the wave growth due to energy input from the wind [*Wright*, 1978; *Alpers and Hasselmann*, 1978]. It has been shown both theoretically and experimentally that for swell conditions, the peak of the small-wave spectrum modulation is no longer at the peak of the long wave, as would be the case if this effect were ignored. In this paper an attempt is made to include this effect. A second effect ignored by the weakly nonlinear model is the presence of wave breaking. Unfortunately, the understanding of breaking waves has not yet advanced to the point where we may easily include this effect, and we will ignore it here.

The purpose of this paper is to gain a clearer understanding of the physical mechanisms underlying the EM bias. We wish to minimize the number of assumptions, both in the electromagnetic calculations and in the geometry of the modulated surface. This desire has led us to perform a numerical experiment which, while computationally intensive, allows us to minimize the number of assumptions required to obtain the final result. For example, it is possible to treat a non-Gaussian modulated surface without making assumptions about the higher-order cumulants or covariance functions, since they are a natural by-product of the simulated surface.

Because of certain idealizations concerning the ocean surface height spectrum, which we make because of our ignorance about the geometry of very small ocean waves, and also for computational reasons, we do not claim to make exact predictions about the magnitude of the EM bias. However, we hope to retain enough of the underlying physics so that the results presented here will be indicators of the EM bias order of magnitude and the dependence on radar frequency and wind speed. In addition, comparison of these results with experimental observations may give an indication of some key piece of the ocean surface physics which needs to be included for future calculations of the bias.

2. Ocean Surface Model

2.1. *Ocean Spectrum*

Because of computational limitations in our scattering calculations, we are forced to consider surfaces that vary only along one dimension. It is known that for a developed ocean, the gravity wave spectrum is concentrated along the wind direction, so that the one-dimensional approximation for this regime may not be substantially wrong. The smaller gravity-capillary waves, however, have a spectrum that although very poorly known is believed to have a broader angular spread. The idealized spectrum presented here can be only an approximation to the true surface height spectrum. Since for nadir incidence the scattering cross section is dependent on the total slope variance and not on the direction of the waves, it is hoped that the approximation presented here retains the key features of the ocean surface which determine the EM bias.

There are certain well-known observations which we have tried to incorporate in our ocean height spectral model. These are as follows:

1. For frequencies greater than the spectral peak and smaller than approximately 10 times the spectral peak frequency, the ocean wavenumber spectrum is a power law whose slope is -3.5 (the equivalent slope for one-dimensional surfaces is -2.5) [*Donelan et al.*, 1985; *Kitaigorodskii*, 1987; *Phillips*, 1985]. The spectral strength is linearly dependent on the wind speed.

2. The ocean slope variance is roughly linearly dependent on the wind speed [*Cox and Munk*, 1954]. The total slope variance S^2 can be approximated by

$$S^2 = 0.003 + 5.12 \times 10^{-3} U \tag{1}$$

where U is the wind speed measured at 10 m, expressed in meters per second.

3. A few measurements exist of the small-wave spectrum [*Jähne and Riemer*, 1990; *Shemdin et al.*, 1988; *Banner et al.*, 1989]. *Jähne and Riemer* [1990], working in a wave tank, and *Shemdin et al.* [1988], working on an ocean platform, observed the wavenumber spectrum to obey a -3.5 power law, for wavelengths greater than a few centimeters. The spectral strengths were observed to be linearly dependent on wind speed. In their elegant measurements, *Jähne and Riemer* [1990] also observed a steep cutoff for smaller wavelengths, so that the contribution of waves smaller than approximately 0.5 cm could be ignored. This cutoff was independent of wind speed. On the other hand, *Banner et al.* [1989], working with a limited set of stereo photographs, observed a -4.0 power law spectrum whose amplitude was only weakly dependent on wind speed. It is too soon to tell which of these observations represents the general case. In this paper, we have decided to follow the observations of *Jähne and Riemer* [1990] since they have very good resolution and represent a very large data set. It is also not clear how the results of *Banner et al.* [1989] can be reconciled with the *Cox and Munk* [1954] results, or with scatterometer observations of wind speed.

4. When the wave age is close to unity, the peak spectral

frequency k_0 is given approximately by g/U^2, where g is the acceleration of gravity.

It is easy to convince oneself that with a typical value for the Phillips constant, the ocean spectrum cannot be given by a single power law for all frequencies and satisfy the *Cox and Munk* [1954] observations, since for a -3.5 power law, the slope variance will be vastly overestimated. Therefore we postulate that there must be a break in the spectrum, so that the spectral amplitude of the smaller waves is less than that predicted by simply extrapolating the large wave spectrum. Such a spectral break has been predicted on the basis of wave breaking statistics by *Glazman and Weichman* [1989]. A similar change in the spectrum is implicit in the work of *Donelan and Pierson* [1987] and *Durden* [1985]. The exact location of the spectral break is not well known. A clue is given, however, by the fact that it has yet to be observed by either spectral measurements of large gravity waves (which cover wavelengths larger than approximately 10 m), or measurements of small waves (covering wavelengths smaller than approximately 2 m). *Glazman and Weichman* [1989] have postulated a break in the spectrum at 3-m wavelength, and we adopted this value.

In order to satisfy all of the previous observations, we chose a spectral model of the form

$$F(k) = k^{-2.5}[s_1 e^{-k/k_1} + s_2 e^{-k/k_2}] \qquad k > k_0 \tag{2}$$

$$k_0 = g/U^2 \tag{3}$$

$$k_1 = 2\pi/3 \text{ m}^{-1} \tag{4}$$

$$k_2 = 2\pi/0.02 \text{ m}^{-1} \tag{5}$$

The spectral strengths s_1 and s_2 are chosen so that the spectrum may satisfy simultaneously equation (1) and the condition

$$F(k_0) = 2.25 \times 10^{-3} \frac{U}{g^{1/2}} k_0^{-2.5} \tag{6}$$

where the strength of the Phillips constant, 2.25×10^{-3}, is obtained from the data of *Kahma* [1981]. Figure 2*a* plots this spectrum for three values of wind speed, while Figure 2*b* plots s_1 and s_2 as a function of wind speed. Notice that the strength of the large-scale waves increases more rapidly with wind speed than does the small-wave strength, but both parameters vary approximately linearly with wind speed, in agreement with experimental results.

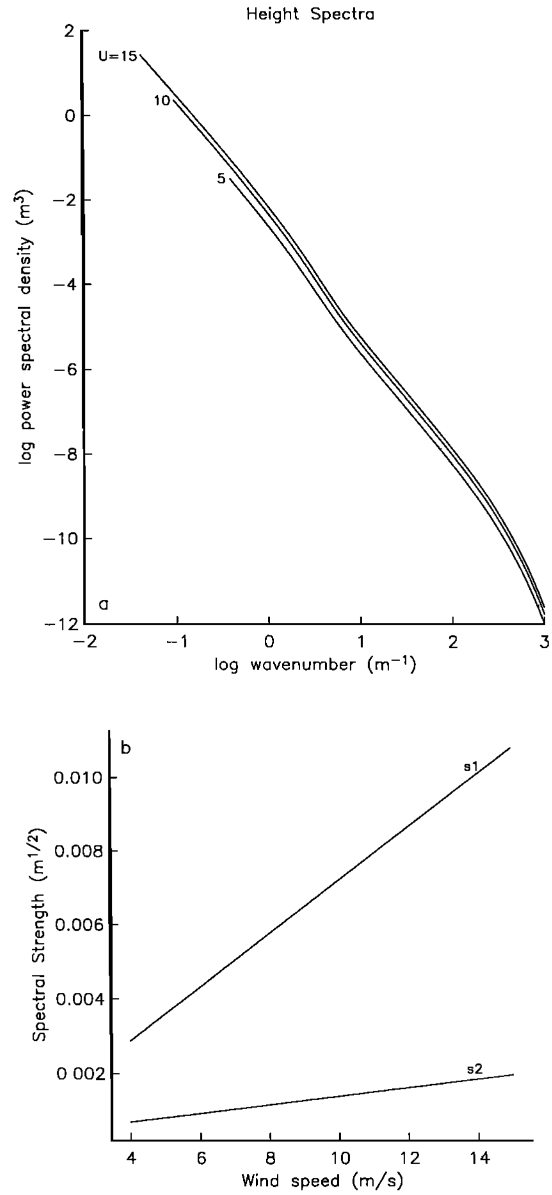

Fig. 2. (*a*) Plot of the ocean spectrum used in this paper for three values of wind speed. (*b*) Spectral strengths for the large waves (s_1) and the small waves (s_2). Note that both depend linearly on wind speed, with s_1 showing much stronger dependence.

2.2. *Large-Scale Wave Field Simulation*

The large-scale wave field has two effects on the small wave patches: the modulation discussed above, and a tilting of the patch relative to the surface normal. This second effect can also have an impact on the EM bias. If the surface tilt variance varies with height, this also may modulate the scattering cross section as a function of height. In order to distinguish between these two mechanisms, we simulated large-scale surfaces with and without this tilt modulation.

Large-scale Gaussian surfaces, which do not exhibit this modulation, were simulated by performing the summation

$$\xi_{\text{linear}}(x, t) = \sum_i z_i \cos \psi_i \tag{7}$$

$$\psi_i = k_i x - w_i t + \phi_i \tag{8}$$

where ξ is the large-scale surface height, z_i is a Rayleigh-distributed random variable whose variance is chosen such that the surface satisfies equation (2), and ϕ_i is a uniformly distributed in the interval $[0, 2\pi]$. The summation was taken over all wave vectors in the large-scale regime, and the spectrum was discretized in small frequency intervals.

In order to include tilt modulation, weakly nonlinear ocean surfaces were generated following *Longuet-Higgins* [1963]:

$$\xi_{\text{nonlinear}} = \xi_{\text{linear}} + \sum_{i,j \le i} z_i z_j [c_{ij} \cos \psi_i \cos \psi_j + s_{ij} \sin \psi_i \sin \psi_j] \tag{9}$$

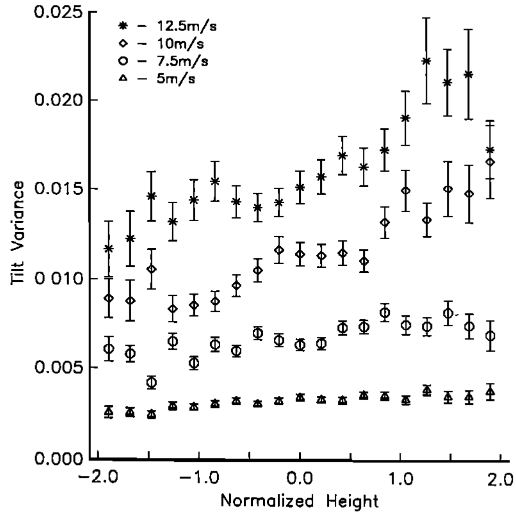

Fig. 3. Large-scale surface tilt variance modulation as a function of wind speed obtained from the Monte Carlo simulation. The error bars show the standard deviation of the simulation results about the reported means. Notice increased modulation with increased wind speed.

where the coupling parameters are given by *Longuet-Higgins* [1963] (after correction for a factor of 1/2).

Theoretically [*Jackson*, 1979], [*Srokosz*, 1986], it can be shown that the slope variance and surface height exhibit a positive correlation. This is confirmed in Figure 3, which presents a plot of the large-scale surface slope variance as a function of height for various wind speeds. In addition to showing the positive correlation, Figure 3 shows that the large-scale slope variance is approximately linearly modulated with wave height and that the degree of modulation increases with wind speed.

2.3. *Small-Wave Modulation*

The modulation of small waves by large waves is a subject of much current research. A WKB approach, based on the conservation of wave action, seems to offer the greatest promise of handling this problem for both gravity and capillary waves [*Alpers and Hasselmann*, 1978], [*Henyey et al.*, 1988]. In this work, we assume that the modulation transfer concept applies [*Alpers and Hasselmann*, 1978]; i.e., the modulation can be calculated linearly from the spectral strengths (see below), and higher-order nonlinear terms are ignored. *Hwang and Shemdin* [1990] have shown that the level of modulation obtained by this approximation agrees very well with a numerical solution of the action conservation equation, for cases involving the modulation of a continuous spectrum by one large-scale wave. Under this approximation, the spectral modulation of the small waves, $\delta F(k)$, can be written as

$$\delta F(k) = F(k)\int dk_L\, z(k_L)R(k,\, k_L)e^{i(k_L x - w_L t)} \tag{10}$$

where $z(k_L)$ is the large-wave complex spectral amplitude, ω_L is the large-wave angular frequency, and the integral is taken over the large-wavelength components. The modulation transfer function $R(k,\, k_L)$ is given by

$$R(k,\, k_L) = \frac{w_L - i\mu}{w_L^2 + \mu^2}\,\frac{w_L}{|k_L|}\,kk_L\left[\frac{k_L}{F(k)}\,\frac{\partial F(k)}{\partial k} - \gamma\,\frac{k_L}{k}\right] \tag{11}$$

$$\gamma = \frac{1}{2}\,\frac{1 + 3(\tau k^2/\rho g)}{1 + \tau k^2/\rho g} \tag{12}$$

where τ is the surface tension and ρ is the density of water. The parameter μ is the growth rate due to the wind. In this paper we have used a form for μ which is the one dimensional analog to the one derived by *Plant* [1982]

$$\mu(k) = 0.04w(k)\left(\frac{u_*}{c(k)}\right)^2 \tag{13}$$

where $c(k)$ is the wave phase velocity, and u_* is the friction velocity. We have assumed that the friction velocity is related to the 10-m wind velocity through the drag coefficient given by *Large and Pond* [1981]. We have assumed neutral stability conditions when calculating the drag coefficient.

The separation of the continuous ocean spectrum into small- and large-wave components is not well defined. Typically, it is assumed that the small-wave wavenumbers are 5 to 10 times greater than the wavenumber of the shortest modulating wave [*Plant*, 1986; *Hasselmann et al.*, 1985]. In this work we have chosen a factor of 5 for the large-small scale separation. There are arguments [*Henyey et al.*, 1988] suggesting that the modulation results should not be a strong function of this value.

EM bias experiments have estimated the bias by illuminating a small (meter scale) patch of the ocean surface and simultaneously recording its mean height to obtain a record of the ocean backscattering cross section as a function of height above the mean sea level. To simulate this situation, we have selected the separation between small and large waves to be 1 m. We have generated realizations of the large scale wave field (see below for more details) and used these realizations together with equations (10) and (2) to obtain the modified spectrum for the small-scale waves for each of the surface patches contained in each realization.

From equations (10) and (9), one can easily obtain the correlation between the small-scale surface height variance σ^2 and the height of the large-scale surface:

$$\langle \xi\sigma^2\rangle = \int_{k_{\text{sep}}}^{\infty} dk_1\, F(k_1)\int_0^{k_1/5} dk_2\, F(k_2)\ \mathrm{Re}\ (R(k_1,\, k_2)) \tag{14}$$

where k_{sep} is the separation wavenumber between large and small scale surfaces. It follows from equation (11) that this is a positive quantity. The Monte Carlo results bear this out and provide details of the shape of the modulation curve. Figure 4 presents the modulation of standard deviations of the small height and slope as a function of height above the mean sea surface (normalized by the total surface standard deviation), for four values of wind speed. As can be seen, there is a substantial, nearly linear, modulation of these quantities as a function of height above the mean sea surface. It will be seen below that this modulation is a major factor in determining the EM bias.

For our purposes, the major effect of the wind growth term is in providing a correlation between the small-scale surface height variance and the large-scale surface tilt, ξ_x

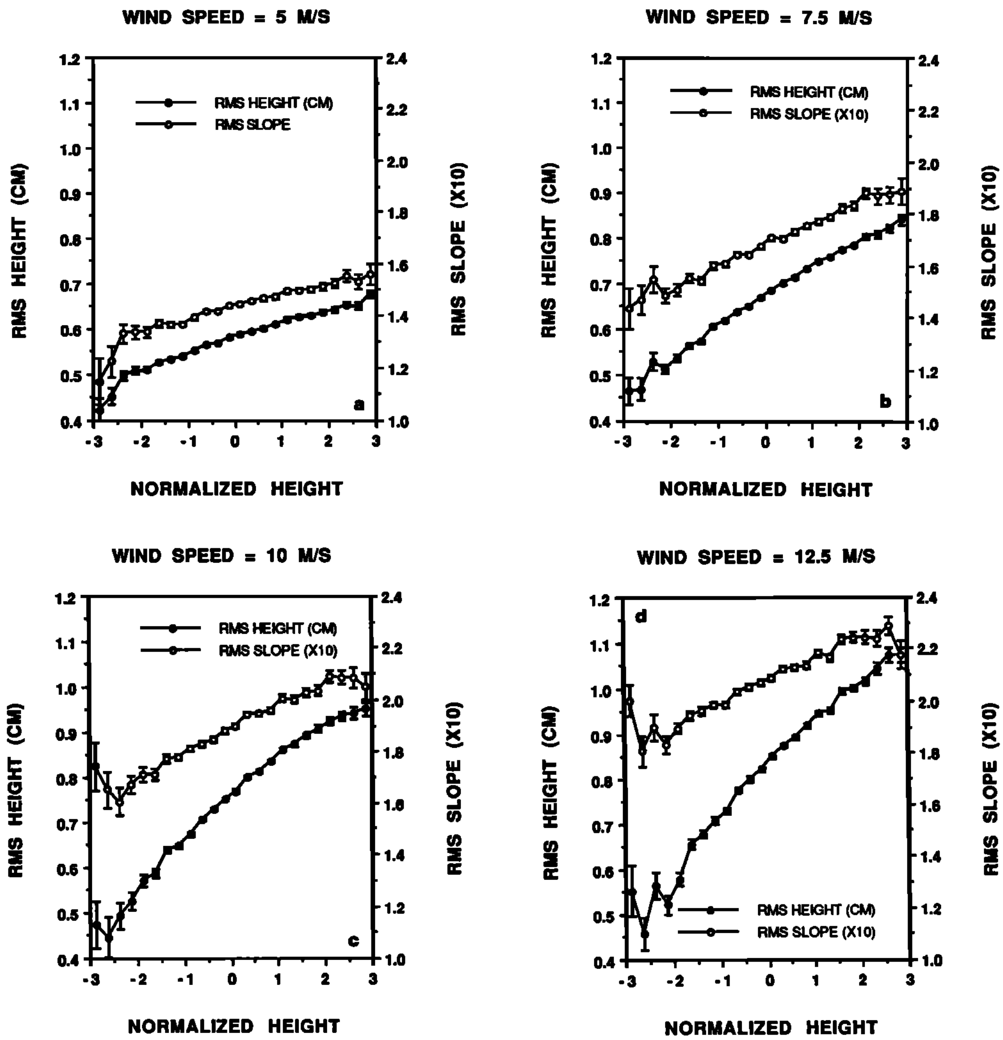

Fig. 4. Modulation of small scale surface height and slope for wind speeds of (*a*) 5 m/s, (*b*) 7.5 m/s, (*c*) 10 m/s, and (*d*) 12.5 m/s from the Monte Carlo simulation. The error bars show the standard deviation of the simulation results about the reported means. Notice the almost linear dependence with normalized surface height, defined as height above mean sea level divided by the surface height standard deviation.

$$\langle \xi_x \sigma^2 \rangle = \int_{k_{\text{sep}}}^{\infty} dk_1 \ F(k_1) \int_0^{k_1/5} dk_2 \ k_2 F(k_2) \ \text{Im} \ (R(k_1, k_2)) \tag{15}$$

Examination of equation (10) shows that this is a negative correlation, so that small-scale surface heights tend to be higher for negative tilts. The Monte Carlo simulation also bears this out and shows that the shape of the modulation is also nearly linear with surface tilt. This phenomenon will skew the brightness of the ocean as a function of tilt but will not be a major contributor to determining the magnitude of the EM bias.

3. Scattering Simulation

We simulated an EM bias experiment by calculating the backscattering cross section as a function of height by generating 50 random independent Gaussian realizations of the small-scale surface, for each of the small surface patches in a large scale surface realization. The spectrum for these realizations is the modulated spectrum, as described above, and the local incidence angle is determined by the large-scale surface slope at the center of that small-wave patch. The large number of realizations is needed to reduce speckle noise for each small-scale patch, so that the mean backscatter cross section may be calculated to an accuracy greater than 0.5 dB. (The accuracy of the mean cross section for a given height bin will be much greater, since the random error will decrease with averaging.) For each wind speed considered, 40 large-scale wave realizations were generated; each realization had a length of 256 m. Thus for each value of wind speed, 512,000 independent scattering calculations were made.

Given the small-scale surface height for each realization, it is possible, in principle, to calculate the induced surface electric current, and subsequently the scattered electromagnetic field, from a simulated radar system with a finite antenna pattern. One possible method of performing this calculation is to use the method of moments (MOM) [*Harrington*, 1968; *Axline and Fung*, 1978], but the computational burden is too great for our computing resources.

An alternative approach is to use an approximate scatter-

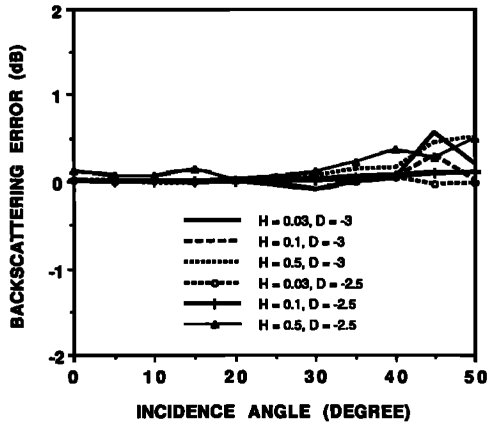

Fig. 5. Error in the UPM backscatter cross section as a function of incidence angle, surface height rms to electromagnetic wavelength ratio (H), and surface spectrum slope (D).

ing theory which agrees well with the MOM results for the particular incidence angles and surface roughness considered and which is computationally more efficient. We have introduced such a theory for perfectly conducting surfaces [*Rodriguez and Kim*, 1991; *Rodriguez et al.*, 1992; *Kim et al.*, 1992], which we call the unified perturbation theory (UPM). We have conducted extensive comparisons of this theory with MOM for oceanlike rough surfaces whose roughness far exceeds the ones considered here. Figure 5 presents a comparison of the performance of the two methods for various incidence angles and for horizontal polarization (electric field parallel to the ocean wave crests, for one-dimensional surfaces). It can be seen that this theory provides excellent agreement with MOM for all incidence angles considered. We have therefore chosen the UPM theory as an accurate alternative to MOM.

The numerical implementation of the theory for random rough surfaces is presented by *Rodríguez et al.* [1992] and *Kim et al.* [1992], and we refer the reader to these references for the details of the scattering calculation. We simulate a Gaussian antenna pattern to limit the scattering area to the small wave patch and calculate the scattered field for a horizontally polarized incident field, and for incident wavelengths of 2 (K_u band) and 5 (C band) cm. These wavelengths are close to the ones to be used by the TOPEX (Topographic Experiment) altimeter and the ones used by past altimeter systems. Given the scattered fields calculated for the 50 small-scale realizations, the scattered power is calculated by averaging the return power from each patch, normalized by the patch length, and the result is recorded together with the small-scale height and tilt variations.

The effect of the large-scale surface on the scattering calculation is only to provide the local incidence angle, and we have neglected the effect of large-scale surface curvature on the small patch. In this sense, we are dealing with a two-scale theory. However, this should not be confused with the conventional electromagnetic two-scale theories [*Hasselmann et al.*, 1985], where the separation between large- and small-scale surfaces occurs at a length typically of the same size as the electromagnetic wavelength. Our two-scale separation is made on other grounds, and the UPM theory does not need the introduction of an additional arbitrary electromagnetic parameter.

In order to obtain a comparison with the geometric optics theory and to obtain the EM bias for very small radar wavelengths, we also calculate the deep phase-scattering cross section for each of the small surface patches. For one-dimensional surfaces, this cross section is given by [*Durden*, 1986]

$$\sigma_0 = \left(\frac{\pi}{2}\right)^{1/2} \frac{1}{s \cos^3 \theta} \exp\left[\frac{-\tan^2 \theta}{2s^2}\right] \tag{16}$$

where θ is the local incidence angle and s^2 is the small-scale surface slope variance.

Note that given the same value of slope variance, one-dimensional surfaces will be darker than two-dimensional surfaces because the latter's cross section is dependent on the inverse of the slope variance, not the inverse of the slope standard deviation. Similar considerations imply that given a change in the rms slope with height above the mean sea level, the predicted cross section modulation, and hence the EM bias, will be greater for an isotropic spectrum than for a unidirectional spectrum. Since observational evidence suggests that the high-frequency wave height spectrum is closer to isotropic than unidirectional, we expect that the numerical results presented here will underestimate the magnitude of the EM bias while preserving the overall trends in its behavior.

4. SIMULATION RESULTS

Figure 6 presents scatter plots comparing the UPM scattering cross section with the deep phase cross section for the two frequencies considered and for low and moderate values of the wind speed. It can be seen that the deep phase theory underestimates the scattering cross section for large values of the cross section while overestimating it for low values. As expected, the 2-cm radar cross section agrees with the geometrical optics results better than the 5-cm cross section.

Figure 7*a* presents the average scattering cross section for the two frequencies considered and for the deep phase approximation. Figure 7*b* presents a similar plot, but with the nonlinear surface term removed. As expected, the mean cross section decreases monotonically with wind speed, and the 2-cm (K_u band) cross section is closer to the deep phase cross section than is the 5-cm (C band) cross section. The magnitude of the cross section is lower than experimental measurements [*Melville et al.*, 1991]. This is a result of using a one-dimensional spectrum for the small-scale waves, as was mentioned above. A surprising result is that when the nonlinear surface terms are included, the mean cross section increases. This can be understood as being due to the combination of two effects: the flatter surface patches occur in the wave troughs, where the large scale surface tilt is also smallest. This causes these flatter, and hence brighter, patches to reflect more in the backscatter direction.

Figure 8 presents the mean value of the scattering cross section binned against normalized surface height for the frequencies and wind speeds considered here. For the sake of comparison, the scattering cross sections have been divided by the mean value of the cross section. The error bars (shown for C band only, to avoid clutter) represent the standard error; their magnitude is not a strong function of frequency. The modulation of radar brightness with the height above mean sea level can clearly be seen from these

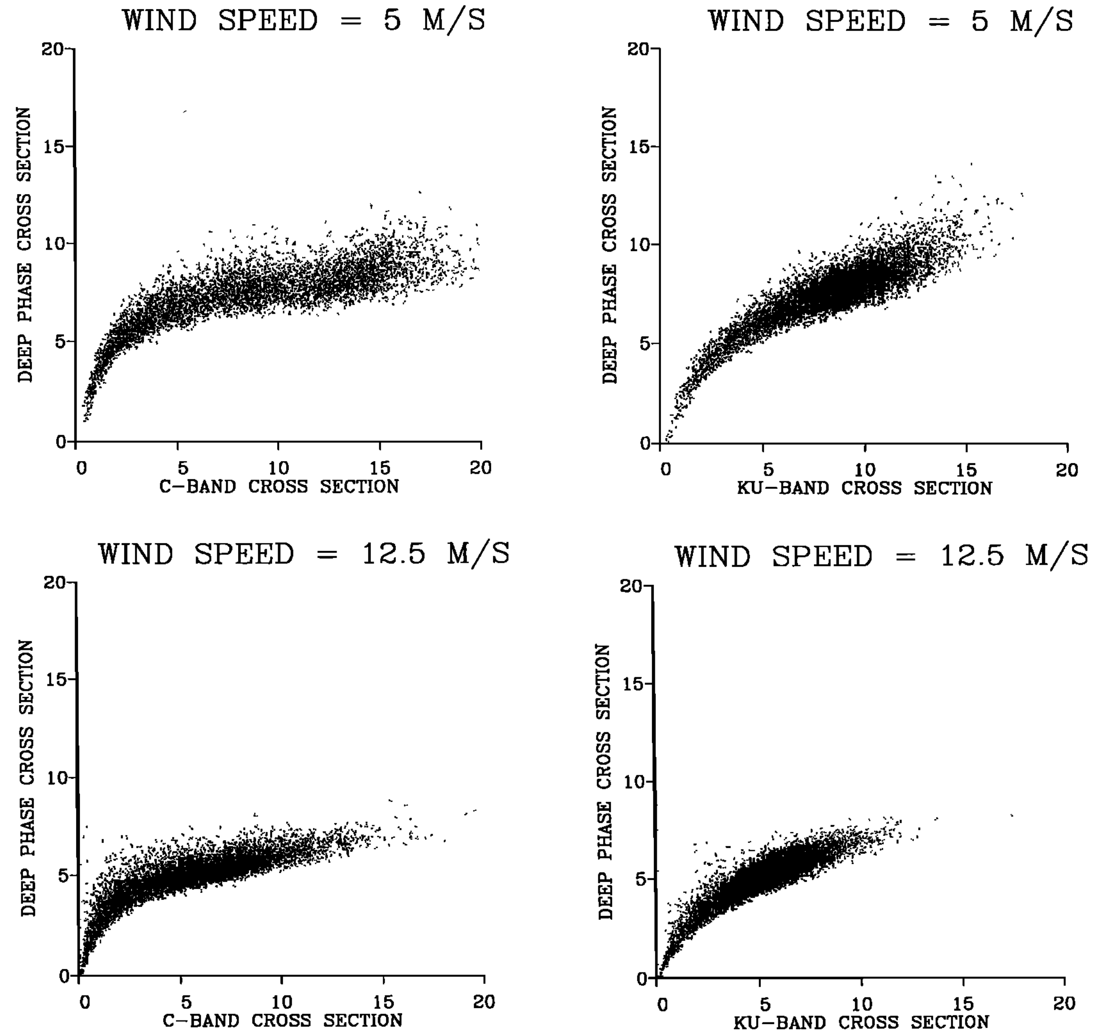

Fig. 6. Scatter plot of the estimated cross sections versus the deep phase approximation for C band and K_u band and two wind speed cases.

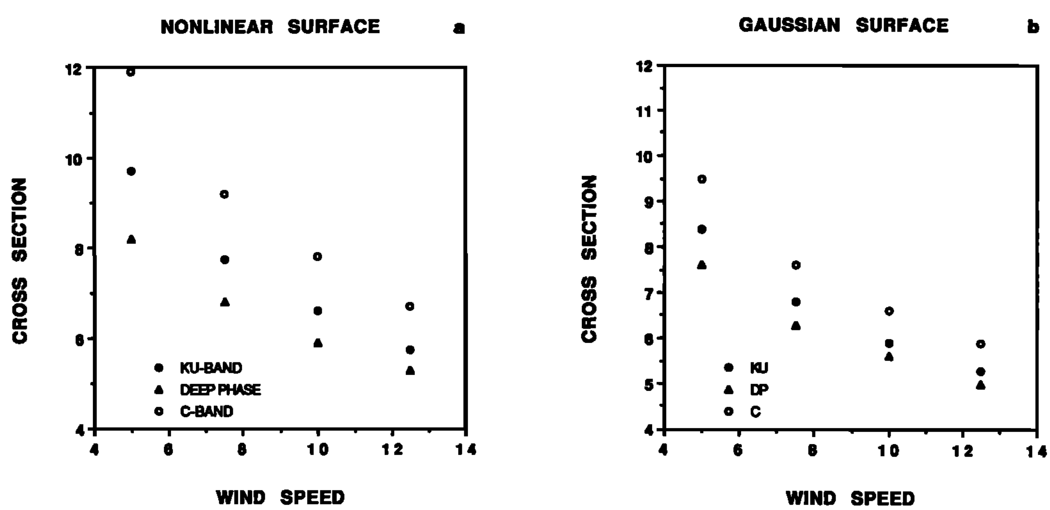

Fig. 7. Comparison of the mean backscatter cross section as a function of wind speed for C band (5-cm wavelength), K_u band (2-cm wavelength), and the deep phase approximation.

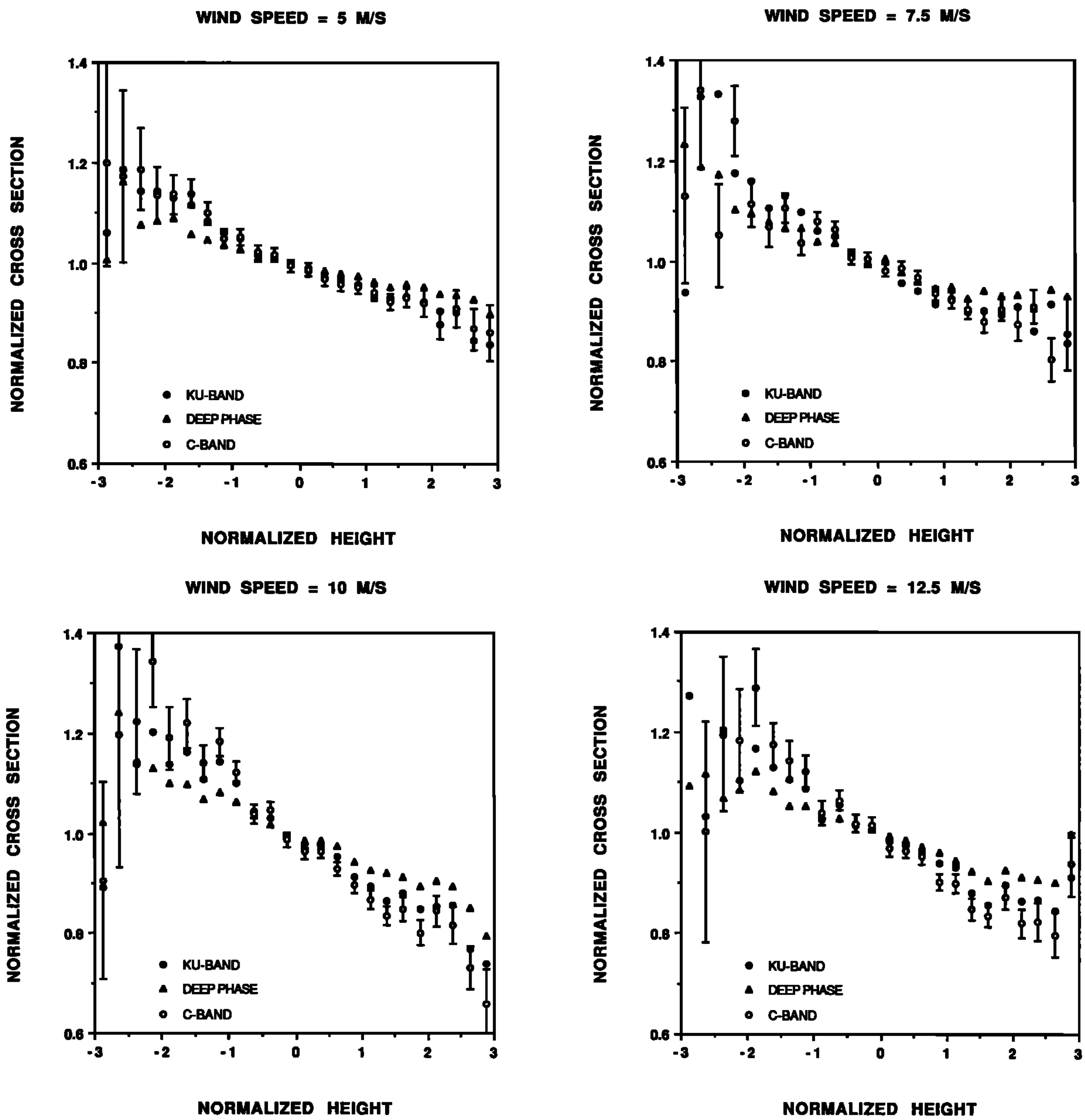

Fig. 8. Modulation of the normalized scattering cross section as a function of wind speed for C band (5-cm wavelength), K_u band (2-cm wavelength), and the deep phase approximation.

figures. The trend in the brightness modulation is similar to that obtained by EM bias experiments [*Yaplee et al.*, 1971; *Walsh et al.*, 1989; *Banner et al.*, 1989]. It is also clear that the shape of this modulation closely follows the linear trend in the modulation of height and slope variance, and differential tilting, presented in Figures 3 and 4. These plots show that the deep phase theory predicts a smaller degree of modulation than the UPM results. The difference between C and K_u band is not as clear, but there seems to be an indication that the C band results show a slightly larger modulation.

To quantify the foregoing conclusion, we calculated the magnitude of the electromagnetic bias for each of the surface types considered. The magnitude of the EM bias is given by the average

$$\delta z_{\mathrm{EM}} = \frac{\langle \xi \sigma_0(\xi) \rangle}{\langle \sigma_0(\xi) \rangle} \tag{17}$$

where angular brackets represent ensemble averaging, ξ is the surface height above mean sea level, and $\sigma_0(\xi)$ is the scattering cross section as a function of surface height. The results for both Gaussian and non-Gaussian large-scale surfaces are presented in Figure 9.

Figures 9*a* and 9*b* show that the bias is negative and that its magnitude increases with SWH, in agreement with experimental results. However, the magnitude of the bias seems to be smaller, by a factor of 2, from the experimental results obtained by *Melville et al.* [1991]. It may be that this discrepancy is due to the specific spectral assumptions made here. As expected, the nonlinear surface exhibits a greater

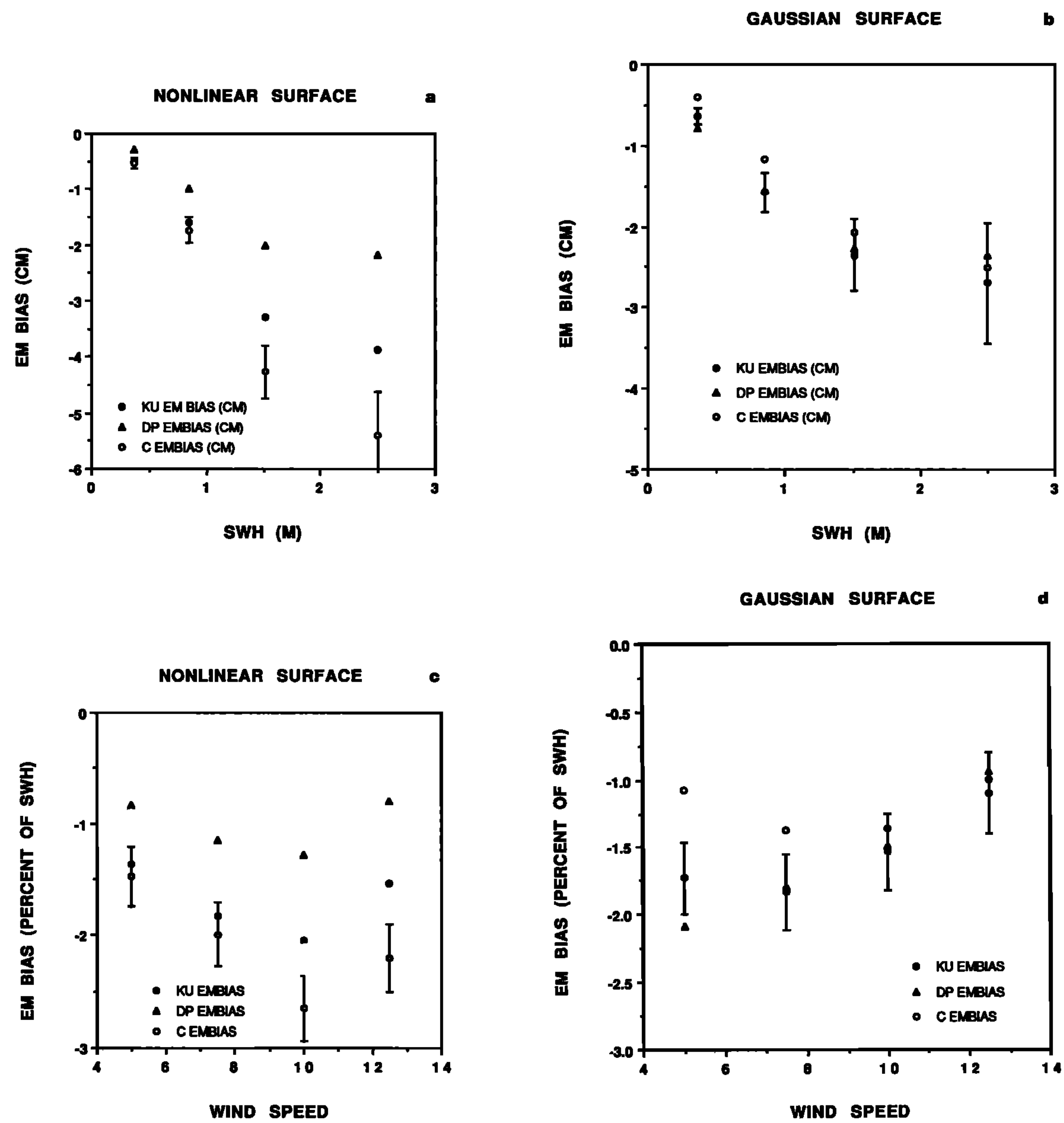

Fig. 9. EM bias as a function of SWH for (*a*) modulated surfaces and (*b*) Gaussian surfaces (note the nearly linear dependence), and EM bias divided by SWH as a function of wind speed for (*c*) modulated and (*d*) Gaussian surfaces. Notice that this residual bias also increases with both increasing wind speed and electromagnetic wavelength.

bias, due to the tilt variance modulation. Assuming that the two effects can be considered as additive (which should be the case, since they are independent, small perturbations), it can be seen that both the modulation of small waves and the modulation of large-scale surface tilt contribute roughly the same amount to the bias. For small values of the bias, the C band and K_u band biases are nearly equal, but the C band bias is greater for larger values of the bias. This agrees qualitatively with the results obtained by *Melville et al.* [1991]. On the other hand, the deep phase modulation is always less than the other two and is approximately 1% of significant wave height. This result agrees very well with the observations of *Walsh et al.* [1989], which were conducted using a K_a band radar (0.8-cm wavelength), for which the deep phase approximation should apply.

The electromagnetic frequency dependence of the EM bias may be better understood if we consider a plot of the dependence of the normalized cross section as a function of surface tilt, Figure 10 (which is typical for all wind speeds). In this figure we can see that the lower-frequency cross section is more deeply modulated by surface tilt, and the deep phase cross section exhibits the least modulation. (The lack of symmetry of the cross section with incidence angle can be explained in terms of the correlation of small-scale roughness and large-scale slope, discussed above.) This can be understood by recalling that as surfaces become very rough, compared with the radar wavelength, their angular scattering approaches a Lambertian (or angular independent) pattern. Since the average cross section for a given height represents an average over all surface tilts, the tilt dependence of the radar cross section will partly determine this mean value. Recalling that the tilt variance is modulated, and that the degree of modulation increases with wind speed, one would expect that the modulation of the cross section

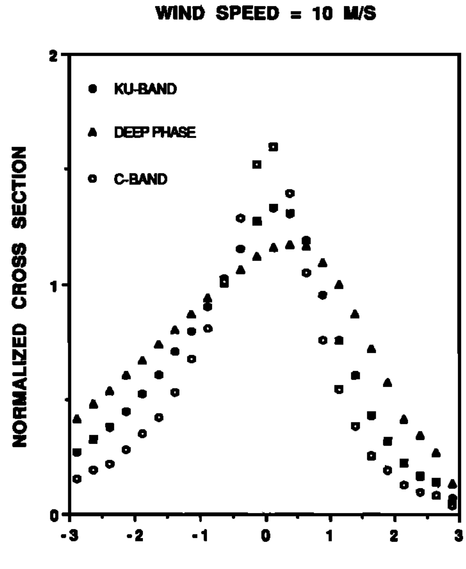

Fig. 10. Normalized scattering cross section as a function of large wave tilt for C band (5-cm wavelength), K_u band (2-cm wavelength), and the deep phase approximation. The wind speed is 10 m/s. The greater sensitivity of the cross section with increasing wavelength accounts for the wavelength (or frequency) dependence of the EM bias.

with frequency would increase with increasing wind speed. For low values of the wind speed, one would then expect the least frequency dependence in the EM bias, whereas the frequency dependence would be greatest at higher wind speeds. This is indeed the observed trend.

After normalizing the bias with the significant wave height, effectively removing a linear trend, the residual normalized bias still exhibits a trend with wind speed for the nonlinear surfaces, but only a slight, and opposite, trend for the Gaussian surfaces. This is due to the fact that the tilt variance modulation increases with wind speed, while the small-scale modulation increases more slowly than the significant wave height. For the nonlinear surfaces, the bias magnitude tends to increase linearly with wind speed up to 10 m/s and then exhibits a slight decrease for the higher wind speeds. The magnitude of the normalized bias roughly doubles over this interval, which is also in agreement with the results of *Melville et al.* [1991]. E. J. Walsh et al. (personal communication, 1991) have observed experimentally the decrease in wind speed dependence for wind speeds above 10 m/s. The same phenomenon can be read into the *Melville et al.* [1991] data, but there are not enough points to make a convincing determination.

5. CONCLUSIONS

We have conducted a numerical experiment to examine the physical mechanisms underlying the EM bias. While we have considered an idealized case, we believe that the conclusions reached here give valuable insights about the nature of the EM bias and perhaps future steps that need to be included in the modeling of the EM bias.

The following list summarizes our conclusions:

1. Conservation of wave action, in the modulation transfer approximation, predicts a modulation of the small-wave spectrum which is approximately linear with surface height. This includes the contribution from both gravity and capillary waves.

2. The large-scale tilt variance is also modulated linearly when weakly nonlinear wave-wave interactions are introduced.

3. On a patch by patch basis, the deep phase approximation does not predict the correct scattering cross section for either of the frequencies considered. The deep phase approximation also tends to underestimate the scattering cross section modulation, especially for nonlinear surfaces.

4. The cross section modulation is nearly linear with surface height, in agreement with the experimental results of *Banner et al.* [1989] but in disagreement with the results of *Walsh et al.* [1989].

5. The sign of the EM bias agrees with experimental observation. The one-dimensional spectral model used underestimates the EM bias by roughly a factor of 2. However, the frequency dependence of the bias is in general in agreement with the results of *Melville et al.* [1991] and *Walsh et al.* [1989]. The same can be said of the bias wind speed dependence, which was shown to be due to the increased modulation of large surface tilt as a function of wind speed.

6. The EM bias is due to two mechanisms: the modulation of small scale waves, and the tilt modulation due to the large waves. Both mechanisms have roughly equal importance. The frequency dependence of the EM bias is explained in terms of the sensitivity of radar cross section to surface tilt and the modulation of tilt variance.

We have presented a model of the EM bias which exhibits trends that are quite similar to those observed in real data, and which clarifies the nature of the cross section modulation. In particular, the mechanisms which govern the radar frequency and wind speed dependence of the bias were elucidated. It remains to be shown in future work whether by adopting a more realistic spectral model, one may also obtain the exact magnitude of the EM bias from similar scattering calculations. We conclude that the greatest unknown, at this time, in modeling of the EM bias is the detailed form of the two-dimensional capillary-gravity wave spectrum and the inclusion of wave breaking effects.

Acknowledgments. The research described in this paper was performed by the Jet Propulsion Laboratory, California Institute of Technology, under contract with the Office of Naval Research.

REFERENCES

Alpers, W. R., and K. Hasselmann, The two-frequency microwave technique for measuring ocean-wave spectra from an airplane or satellite, *Boundary Layer Meterol.*, *13*, 215–230, 1978.

Arnold, D. V., J. A. Kong, and W. K. Melville, Physical optics prediction of EM bias, paper presented at Progress in Electromagnetic Research Symposium, Boston, Mass., 1991.

Axline, R. M., and A. K. Fung, Numerical computation of scattering from a perfectly conducting random surface, *IEEE Trans. Antennas Propag.*, *AP-26*, 482–488, 1978.

Banner, M. L., I. S. F. Jones, and J. C. Trinder, Wavenumber spectra of short gravity waves, *J. Fluid Mech.*, *198*, 321–344, 1989.

Barrick, D. E., and B. J. Lipa, Analysis and interpretation of altimeter sea echo, *Adv. Geophys.*, *27*, 61–100, 1985.

Cox, C., and W. Munk, Statistics of the sea surface derived from sun glitter, *J. Mar. Res.*, *13*, 198–227, 1954.

Donelan, M. A., and W. J. Pierson, Radar scattering and equilibrium ranges in wind-generated waves with application to scatterometry, *J. Geophys. Res.*, *92*(C5), 4971–5029, 1987.

Donelan, M. A., J. Hamilton, and W. H. Hui, Directional spectra of wind-generated waves, *Philos. Trans. R. Soc. London, Ser. A*, *315*, 509–562, 1985.

Durden, S. L., Microwave scattering from the ocean surface, *Sci. Rep. D901-1986-1*, Cent. for Radar Astron., Stanford Univ., Stanford, Calif., 1986.

Durden, S. L., and J. F. Vesecky, A physical radar cross section model for a wind-driven sea with swell, *IEEE J. Oceanic Eng.*, *OE-10*, 445–451, 1985.

Glazman, R. E., and M. A. Srokosz, Equilibrium wave spectrum and sea state bias in satellite altimetry, *J. Geophys. Res.*, in press, 1992.

Glazman, R. E., and P. B. Weichman, Statistical geometry of a small surface patch in a developed sea, *J. Geophys. Res.*, *94*(C4), 4998–5010, 1989.

Harrington, R., *The Method of Moments*, MacMillan, New York, 1968.

Hasselmann, K., R. K. Raney, W. J. Plant, W. Alpers, R. A. Shuchman, D. R. Lyzenga, C. L. Rufenach, and M. J. Tucker, Theory of synthetic aperture radar ocean wave imaging: A MARSEN view, *J. Geophys. Res.*, *90*, 4659–4686, 1985.

Henyey, F. S., D. B. Creamer, K. B. Dsythe, R. L. Schult, and J. Wright, The energy and action of small waves riding on large waves, *J. Fluid Mech.*, *189*, 443–462, 1988.

Hwang, P. A., and O. H. Shemdin, Modulation of short waves by surface currents: A numerical solution, *J. Geophys. Res.*, *95*(C9), 16,311–16,318, 1990.

Jackson, F. C., The reflection of impulses from a nonlinear random sea, *J. Geophys. Res.*, *84*(C8), 4934–4939, 1979.

Jähne, B., and K. S. Riemer, Two-dimensional wave number spectra of small-scale water surface waves, *J. Geophys. Res.*, *95*(C7), 11,531–11,546, 1990.

Kahma, K. K., A study of the growth of the wave spectrum with fetch, *J. Phys. Oceanogr.*, *11*, 1503–1515, 1981.

Kim, Y., E. Rodríguez, and S. L. Durden, A numerical assessment of rough surface scattering theories: Vertical polarization, *Radio Sci.*, in press, 1992.

Kitaigorodskii, S. A., A general explanation of the quasi-universal form of the spectra of wind-generated gravity waves at different stages of their development, *Johns Hopkins APL Tech. Dig.*, *8*(1), 11–14, 1987.

Large, W. G., and S. Pond, Open ocean momentum flux measurements in moderate to strong winds, *J. Phys. Oceanogr.*, *11*, 324–336, 1981.

Longuet-Higgins, M. S., The effect of nonlinearities on statistical distributions in the theory of sea waves, *J. Fluid Mech.*, *17*, 459–480, 1963.

Melville, W. K., R. H. Stewart, W. C. Keller, J. A. Kong, D. V. Arnold, A. T. Jessup, M. R. Loewen, and A. M. Slinn, Measurements of electromagnetic bias in radar altimetry, *J. Geophys. Res.*, *96*(C3), 4915–4924, 1991.

Phillips, O. M., *The Dynamics of the Upper Ocean*, Cambridge University Press, New York, 1980.

Phillips, O. M., Spectral and statistical properties of the equilibrium range in wind-generated gravity waves, *J. Fluid Mech.*, *156*, 505–531, 1985.

Plant, W. J., A relationship between wind stress and wave slope, *J. Geophys. Res.*, *87*(C3), 1961–1967, 1982.

Plant, W. J., A two-scale model of short wind-generated waves and scatterometry, *J. Geophys. Res.*, *91*(C9), 10,735–10,749, 1986.

Rodríguez, E., and Y. Kim, A unified perturbation expansion for surface scattering, *Radio Sci.*, *27*, 79–93, 1991.

Rodríguez, E., Y. Kim, and S. L. Durden, A numerical assessment of rough surface scattering theories: Horizontal polarization, *Radio Sci.*, in press, 1992.

Srokosz, S. A., On the joint distribution of surface elevation and slopes for a nonlinear random sea, with an application to radar altimetry, *J. Geophys. Res.*, *91*(C1), 995–1006, 1986.

Shemdin, O. H., H. M. Tran, and S. C. Wu, Directional measurements of short ocean waves with stereophotography, *J. Geophys. Res.*, *93*, 13,891–13,901, 1988.

Tsang, L., J. A. Kong, and R. T. Shin, *Theory of Microwave Remote Sensing*, Wiley-Interscience, New York, 1985.

Tyler, G. L., Wavelength dependence in radio-wave scattering and specular point theory, *Radio Sci.*, *11*(2), 83–91, 1976.

Walsh, E. J., F. C. Jackson, E. A. Uliana, and R. N. Swift, Observations of electromagnetic bias in radar altimeter sea surface measurements, *J. Geophys. Res.*, *94*(C10), 14,575–14,584, 1989.

Wright, J., Detection of ocean waves by microwave radar: The modulation of short gravity-capillary waves, *Boundary Layer Meteorol.*, *13*, 87–105, 1978.

Yaplee, B. S., A. Shapiro, D. L. Hammond, B. D. Au, and E. A. Uliana, Nanosecond radar observations of the ocean surface from a stable platform, *IEEE Trans. Geosci. Electron.*, *GE-9*, 171–174, 1971.

Y. Kim, J. M. Martin, and E. Rodríguez, Jet Propulsion Laboratory, California Institute of Technology, 4800 Oak Grove Drive, Pasadena, CA 91109.

(Received January 24, 1991;
revised October 2, 1991;
accepted October 2, 1991.)